Materials Today Energy 34 (2023) 101317

Contents lists available at ScienceDirect

Materials Today Energy

journal homepage: www.journals.elsevier.com/materials-today-energy/

Construction of V_2O_x/Si heterojunction and carrier-assisted collection for high-efficiency silicon solar cells

Qi Geng [a], Zhe Wang [a], Zhen Liu [a], Yuzhou Liu [a], Zhongliang Gao [c], Yingfeng Li [a], Xin Sun [a], Lei Chen [b], Xiaojun Lv [a], Meicheng Li [a, *]

[a] State Key Laboratory of Alternate Electrical Power System with Renewable Energy Sources, School of New Energy, North China Electric Power University, Beijing 102206, China
[b] School of Mathematics and Physics, North China Electric Power University, Beijing 102206, China
[c] School of Electrical and Electronic Engineering, Shandong University of Technology, Zibo 255000, China

ARTICLE INFO

Article history:
Received 2 February 2023
Received in revised form
8 April 2023
Accepted 16 April 2023
Available online 20 April 2023

Keywords:
V_2O_x
Si
Heterojunction
PEDOT:PSS
Solar cells

ABSTRACT

Vanadium oxide (V_2O_x) is a typical wide-bandgap transition metal oxides semiconductor, with excellent hole selective contact performance by forming heterocontact with Si. Nevertheless, the poor lateral conductivity of V_2O_x film weakens the carrier collection ability and limits the performance of solar cells. Here, V_2O_x/Si heterojunction was clearly demonstrated and achieved superior carrier separation. Meanwhile, the carrier collection efficiency was enhanced through PEDOT:PSS for accomplishing the power conversion efficiency improvement. The V_2O_x/Si heterojunction was confirmed via Kelvin probe force microscopy with a potential difference in the junction area, and an appropriate work function of V_2O_x film was acquired under low annealing temperature. Numerical simulations also synergistically reveal the role of V_2O_x/Si heterojunction, and the high band bending at Si surface was 0.84 eV, which further promotes carrier separation. Finally, the V_2O_x/Si heterojunction solar cell was fabricated with PEDOT:PSS and showed a power conversion efficiency of 12.64%, which was 6 times higher than basic V_2O_x/Si heterojunction solar cell. These results provide a new reference for fabricating low-cost, technically simple, and high-efficiency solar cells.

1. Introduction

Transition metal oxides (TMOs) have been widely used in crystalline silicon (c-Si) [1–4], perovskite [5–8], polymer [9–11], and organic solar cells [12–15] with the advantages of their suitable energy level and good stability. Among the TMOs, VO_x and MoO_x are served as the hole selective contact layer for c-Si solar cells. At the same time, they also possess a satisfactory surface passivation effect and high work function, in which the power conversion efficiency (PCE) of c-Si solar cells had exceeded 21% [16]. For example, using MoO_x film instead of p-type, a-Si:H layer could significantly reduce parasitic absorption and improve short circuit density, achieving a high PCE of 23.5% in silicon heterojunction solar cells [17]. Recently, vanadium oxide film has shown good stability and low contact resistivity (ρ_c) and has been applied as a hole selective contact layer in n-type c-Si solar cells, obtaining a PCE of 21.6% [18]. A 22.03% PCE was also reached in p-type c-Si solar cell with V_2O_x/SiO_x/NiO_x full area back contact [19].

Usually, some methods are focused on the application of TMOs film as a hole selective contact layer in silicon solar cells [20,21]. However, few studies pay attention to the direct contact between TMOs and Si to construct heterojunction solar cells. Through deposing molybdenum oxide film directly on n-type silicon, an 0.58 V high open circuit voltage (V_{OC}) was displayed due to the high-quality junction, and a corresponding PCE was 4.45% [22]. It also provides a reference for developing high efficiency and low capital TMOs/Si heterocontact solar cells. Whereas, the relatively lower efficiency is attributed to the absence of carrier collection layers. Lately, using V_2O_x film as hole selective contact layer and using ITO layer to increase the carrier collection ability, the silicon solar cell can obtain a PCE of 10.8% [23]. Similarly, through etching silicon nanowires on Si surface and adjusting the length of silicon nanowires, the silicon nanowire solar cells with V_2O_x film and ITO reach a PCE of 12.37% [24]. Nevertheless, the weak lateral conductivity of V_2O_x film impairs the efficient carrier collection and

* Corresponding author.
E-mail address: mcli@ncepu.edu.cn (M. Li).

https://doi.org/10.1016/j.mtener.2023.101317
2468-6069/

further limits the efficiency of the device. Therefore, the assisted carrier collection layer also plays a crucial role in improving performance.

In this work, we fabricated V_2O_x/Si heterojunction by solution methods, avoiding high energy consumption, toxic raw materials, and complicated process. Meanwhile, the potential difference of V_2O_x/Si contact interface clearly indicated the formation of heterojunction. The photoelectronic information and energy band contact properties of V_2O_x film forming heterojunction with Si at different annealing temperatures were obtained. And then, the V_2O_x/Si heterojunction solar cell was fabricated in experiment, and the high efficiency of V_2O_x/Si heterojunction solar cell was also verified by numerical simulation. Furthermore, the assisted layer of PEDOT:PSS was applied to enhance the collection efficiency after carrier separation at the area of V_2O_x/Si heterojunction, which accomplished a PCE of 12.64%.

2. Results and discussion

2.1. Structure design of V_2O_x/Si heterojunction solar cell

In the beginning, the solution of V_2O_x was coated on the n-Si wafer to construct the V_2O_x/Si heterojunction, and the structure of V_2O_x/Si heterojunction solar cell was also shown in Fig. 1(a). In order to elaborate the function of assisted collection carrier layer, Fig. 1(b) shows the route of carrier with and without the assisted carrier collection layer of PEDOT:PSS film. In the absence of assisted carrier collection layer, at the V_2O_x/Si heterojunction region, the inferior lateral conductivity V_2O_x film contact with the Ag electrode directly cannot collect carrier effectively to form a good current after the carrier separation. However, when the assisted collection carrier layer was available, the separated carrier could be collected efficiently and driven them to transport to Ag electrode to achieve the good performance of V_2O_x/Si heterojunction solar cells.

2.2. V_2O_x/Si heterojunction solar cell

After designing the structure of V_2O_x/Si solar cells, we studied the properties of V_2O_x film at different annealing temperatures. The crystal structure of V_2O_x films annealed at 120 °C, 300 °C in the air for 15 min, 1 h, and Si wafer of without annealing was shown in Fig. 2, respectively. The film of V_2O_x was spin coated 15 times on the Si wafer. At 120 °C, the V_2O_x film was presented in amorphous structure with no diffraction peaks. As the annealing temperature increasing, the V_2O_x film becomes crystalline after annealing at 300 °C for 1 h. The pattern of V_2O_x film reveals two peaks at 20.26° and 41.25°, which correspond to (001) and (002) crystal planes, respectively. Furthermore, with the annealing temperature is further increased to 500 °C in Fig. S1(a), the more diffraction peaks were observed. Including more intensity peak of (001) and new peaks of (101) and (301) were spotted for the first time at the diffracted angles at 21.71° and 31.00°, respectively (JCPDS card no. 00-041-1426) [25]. In conclusion, the change of annealing temperature affects the crystalline intensity of V_2O_x films. This was also shown that V in V_2O_x film has a multivalent state at 120 °C annealing temperature. Additionally, the same patterns appear in Raman spectra in Fig. S1(b). Under low temperature, the Raman spectra show no obvious peaks, and the vibrations of V—O and V—O—V were shown visibly until the temperature rises to 300 °C and 500 °C [26,27], which is consistent with the X-ray diffraction (XRD) representation. Scanning electron microscopy (SEM) surface images of V_2O_x film on Si wafer at different annealing temperatures of 120 °C, 300 °C, 500 °C and bare Si were also shown in Fig. S2. It was discovered that the crystalline state of nanostriated was obviously at annealing temperature of 300 °C in Fig. S2(c). When the annealing temperature increased to 500 °C, the discontinuous nanocolumnar crystals appeared in Fig. S2(d). However, in V_2O_x/Si heterojunction solar cell, the crystallized V_2O_x film exhibits poor optoelectronic properties in Fig. S3, which was probably caused by the grain boundary scattering of V_2O_x film [28]; thus, the amorphous V_2O_x film was used in this research.

It has been demonstrated that the V_2O_x film at different annealing temperatures have different patterns, in order to confirm the specific valence state of V_2O_x film, the X-ray photoelectron spectroscopy (XPS) core-level spectra of V 2p and O 1s of the V_2O_x film was also displayed in Fig. 2(b) and (c). The V 2p core level was grouped with double peaks of V $2p_{3/2}$ and V $2p_{1/2}$. When the annealing temperature of V_2O_x film was 120 °C, the binding energies of V $2p_{3/2}$ were splinted into two peaks with a primary peak at 517.5 eV and a small peak at 516.4 eV, which could be attributed to V^{5+} and V^{4+}, respectively [18]. An obvious change is that the amounts of V^{4+} decrease with the annealing temperature increased, until the annealing temperature continues to raise 500 °C, the valence state of vanadium is only V^{5+} in Fig. S2(e). It was illustrated that, as the annealing temperature increases, the valence state of V^{5+} was dominant, which indicates the existence of oxygen vacancy in V_2O_x film prepared by solution methods. In Table 1, the peak area ratio of V^{5+}/V^{4+} was increased from 4.54 to 7.25 with the annealing temperature from 120 °C to 300 °C, corresponding to a decrease in the content of V^{4+}. This was unfavorable to the electrical characteristics of V_2O_x film [24,29]. The V^{4+} could be regarded as an external electron of V^{5+}, and this external electron act as a conductive role for V_2O_x film [30]. Meanwhile, it should be noted that the oxygen vacancy is also an important vehicle, and the carriers could transport validly by these defect states [31].

The work function of V_2O_x film may also be affected by different preparation methods [31,32]; therefore, the V_2O_x films prepared by the whole solution method were characterized by ultraviolet

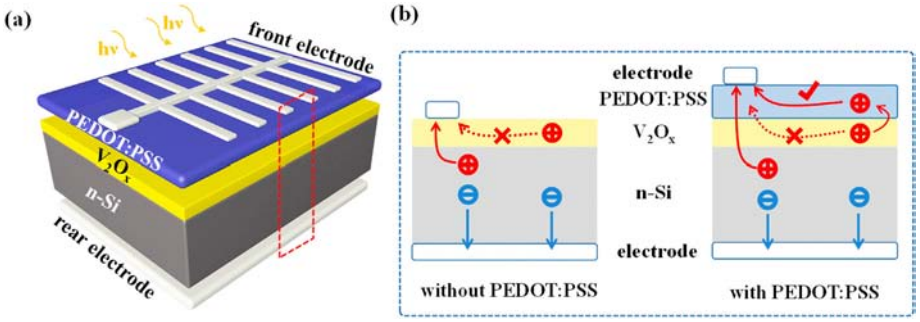

Fig. 1. Structural diagram of V_2O_x/Si heterojunction solar cells. (a) Structure diagram of V_2O_x/Si heterojunction solar cells with PEDOT:PSS film. (b) Schematic diagram of carrier transport in V_2O_x/Si heterojunction solar cells with and without PEDOT:PSS film.

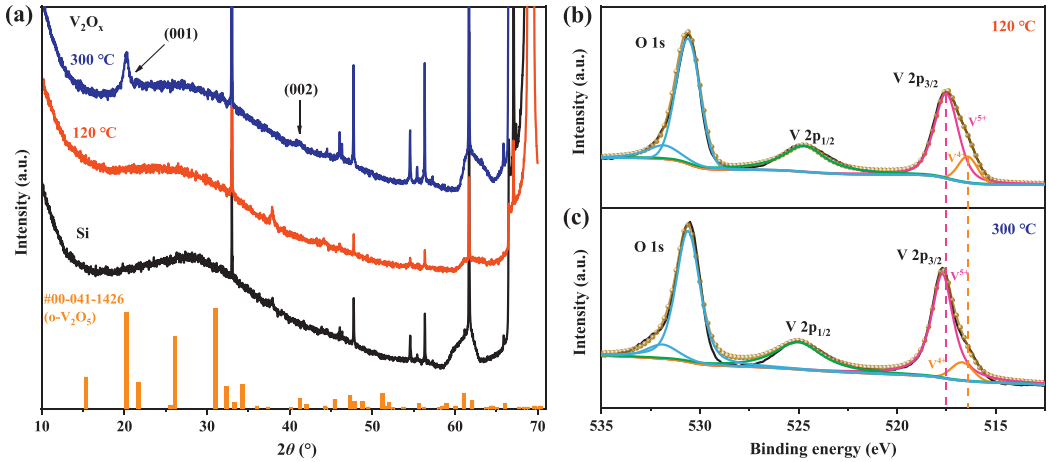

Fig. 2. The crystal and molecular structure of V_2O_x film and X-ray photoelectron spectroscopy (XPS) spectra of O and V of V_2O_x film at different annealing temperatures. (a) X-ray diffraction (XRD) patterns of V_2O_x film annealing at 120 °C for 15 min, 300 °C for 60 min in air and XRD patterns of Si wafer. (b) and (c) XPS spectra of O and V in V_2O_x film at annealing temperatures of 120 °C and 300 °C in air.

Table 1
The peak position and area ratio of V^{5+} and V^{4+} at different conditions.

Temperature	V^{5+}	V^{4+}	V^{5+}/V^{4+}
120 °C	517.5 eV	516.4 eV	4.54:1
300 °C	517.7 eV	516.7 eV	7.25:1

photoelectron spectroscopy (UPS). After obtaining the original data, calibrating, coordinating, transforming, and then calculating by formula (1),

$$\Phi = h\nu - \left(E_{Cutoff} - E_{Fermi}\right) \quad (1)$$

where Φ is work function, hν is incident photon energy, here is 21.2 eV, E_{Cutoff} is the cut-off edge, and E_{Fermi} is the Fermi level after calibration. The work function and valence band maximum (VBM) of V_2O_x films at different annealing temperatures were shown in Fig. 3 of the UPS spectrum. It can be calculated that the conduction band (E_C) of V_2O_x film is 4.86 eV at 120 °C annealing temperature, which obtained from the formula of $E_C = W_F$ (Φ)+VBM-E_g. The values of VBM, W_F, and bandgap (E_g) of V_2O_x film were 2.73 eV 4.93 eV, and 2.8 eV as obtained from Fig. 3(a)–(c). At 120 °C annealing temperature, the transmittance was higher from 300 nm to 650 nm wavelength than 300 °C in Fig. 3(d). In conclusion, the V_2O_x film has good transmittance (above 80%) and suitable bandgap, which is fitted to as a window layer for silicon solar cells. At the same time, we discovered that the work function was increased from 4.93 eV to 5 eV as the annealing temperature improved. Although the value of work function was higher than 120 °C, the performance of V_2O_x/Si heterojunction solar cells was poor. The possible reasons are the grain boundary scattering and unmatched energy level between V_2O_x film and Si. Thus, the suitable work function and matching energy level were very important rather than the higher work function, the better.

Notably, the carrier transportation process and the heterojunction structure were also influenced by work function, so the energy level of V_2O_x film was calculated, and the contact energy level information of V_2O_x/Si heterojunction interface was also shown in Fig. 3. In Fig. 3(e), the energy value from the valence band to the vacuum level is 7.66 eV of V_2O_x film. Meanwhile, when V_2O_x film formed heterojunction with Si, the energy level and carrier separation diagram were also shown in Fig. 3(f). The high work function of V_2O_x film was induced large band bending of Si surface, which accelerate the carrier separation at the V_2O_x/Si heterojunction area. However, the value of valence band to the vacuum level of V_2O_x is higher than Si of 5.15 eV; to a certain extent, it hinders the transportation of carrier from Si to front electrode. Fortunately, since the large difference work function of V_2O_x film and Si, the hole could be concentrated near the bulk trap of valence band interface. And then, the band-to-band (B2B) tunneling or trap-assisted tunneling (TAT) can assist carrier transport smoothly. It is worth noting that different conditions correspond to different tunneling patterns. If the E_C of TMO is greater than the E_V of Si, the B2B is dominant, that is the high work function. Otherwise, the holes may need help through TAT near the valence band area [33]. In this work, although, the work function difference of V_2O_x film and Si is large to induce the band bending of Si to separate carriers. We consider that the value of work function of V_2O_x is not enough to realize the B2B. The TAT of V_2O_x/Si heterojunction interface was happened to accelerate the carrier transport.

After analyzing the properties and energy band information of V_2O_x film, the V_2O_x/Si heterojunction solar cells were fabricated in experiment, and the performance was shown in Fig. 4. Different V_2O_x solution concentrations were used to show the performance of V_2O_x/Si heterojunction solar cells. In Fig. 4(a), the pink line was the Si wafer only contact with the sliver grid electrode, it was found that the I–V curve was a straight line with no any photovoltaic response phenomenon. When the V_2O_x film contacted with Si, the photovoltaic response was obvious, indicating that the carrier was separated by V_2O_x/Si heterojunction and transported to the front electrode to converge into current. But the poor lateral conductivity V_2O_x film could not collect the separated carrier very well, which is the main reason cause the unsatisfied performance. Table 2 shows the electrical output parameters of V_2O_x/Si heterojunction solar cells. At the 1:200 solution concentration (the meaning of 1:150, 1:200 and 1:250 concentration is the volume ratio of V_2O_x and isopropanol) of V_2O_x, the V_{OC} reached 348 mV, and the FF was 60.06%, displaying the best I–V characteristic curve with a PCE about 2.1%. For contact resistance, when the V_2O_x film was inserted between n-Si and Ag, it exhibits an increase in contact resistance due to insulating property of depletion layer in Fig. S4. The width of depletion W_D was 0.9 μm, and the calculation process was shown in supplementary material [24]. At the same time, the reflectivity of different concentration of V_2O_x solution shows the roughly same

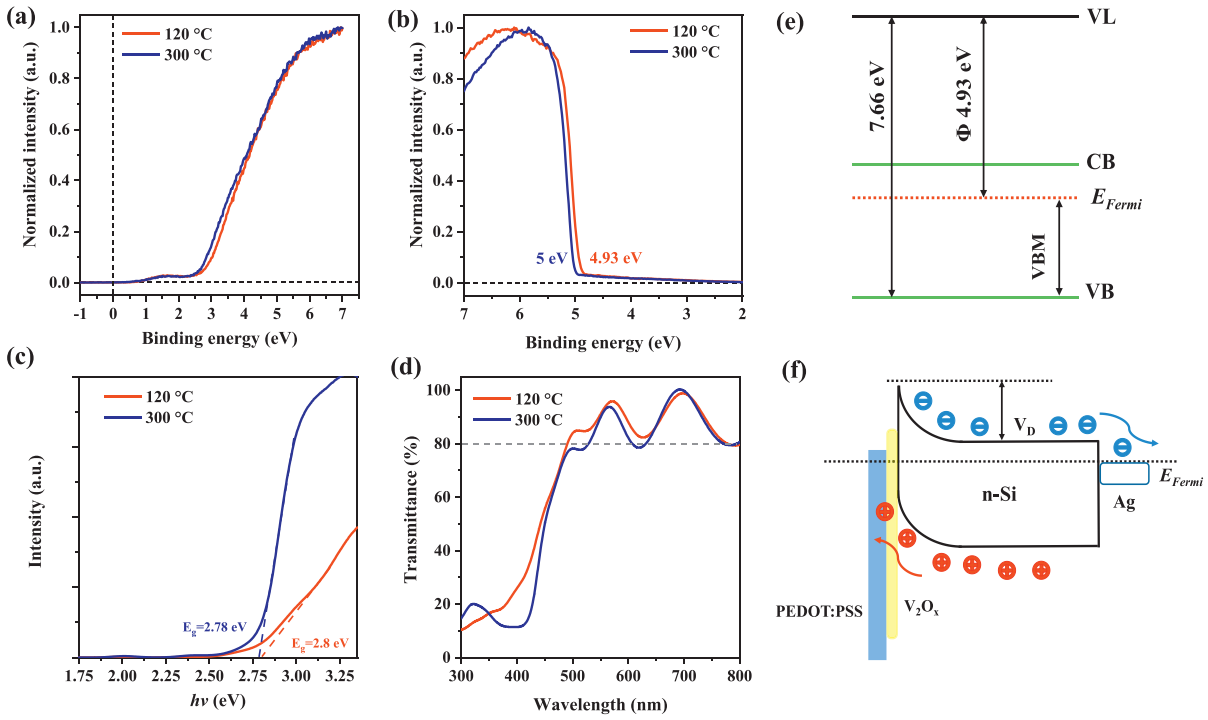

Fig. 3. The photoelectron spectroscopy and schematic diagram of energy level position of V_2O_x film and PEDOT:PSS/V_2O_x/Si. (a) and (b) Ultraviolet photoelectron spectroscopy (UPS) spectra of V_2O_x after coordinate change at annealing temperatures of 120 °C, 300 °C. (c) Bandgap and (d) transmittance spectra of V_2O_x film at annealing temperatures of 120 °C, 300 °C. (e) Schematic diagram for calculating the energy level position of V_2O_x according to UPS spectra and absorption spectrum. (f) Schematic diagram of energy level position and carrier separation of PEDOT:PSS/V_2O_x/Si.

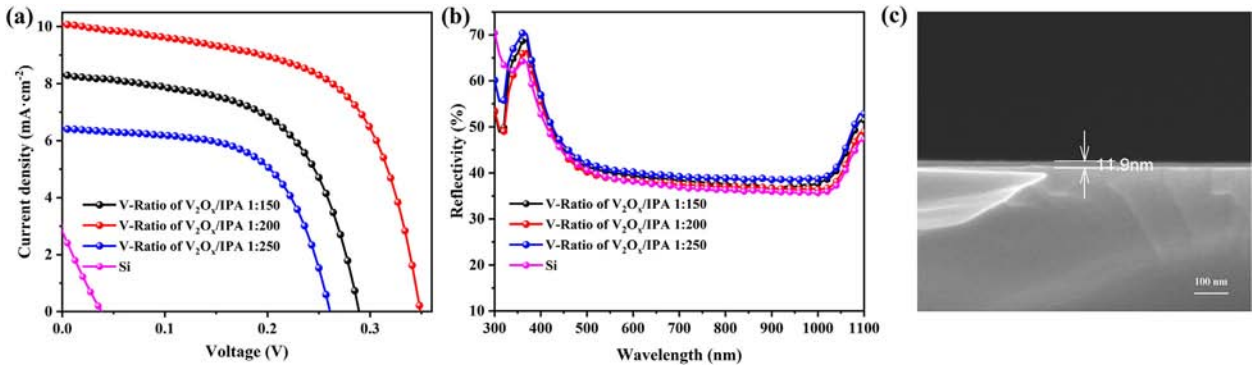

Fig. 4. Performance data of V_2O_x/Si heterojunction solar cells under different V_2O_x solution concentrations and the thickness of V_2O_x film on Si wafer. (a) Current density-voltage curves and (b) reflectivity spectra of V_2O_x/Si heterojunction solar cells under different V_2O_x solution concentrations of 1:150, 1:200, and 1:250. (c) Scanning electron microscopy image of the thickness of V_2O_x film on Si wafer at 1:200 concentration.

Table 2
Electrical output parameters of V_2O_x/Si heterojunction solar cells.

	V_{OC} (mV)	J_{SC} (mA/cm^2)	FF (%)	PCE (%)
1:150	292 (311 ± 21)	8.31 (7.76 ± 0.38)	57.12 (59.19 ± 1.52)	1.38 (1.43 ± 0.12)
1:200	348 (320 ± 29)	10.08 (9.88 ± 1.34)	60.06 (60.19 ± 1.53)	2.10 (1.89 ± 0.15)
1:250	264 (252 ± 10)	6.42 (6.02 ± 0.37)	60.27 (60.44 ± 0.23)	1.02 (0.92 ± 0.09)

*The data in parentheses are calculated by five sets of solar cells.

trend in Fig. 4(b) but higher than that of Si wafer. Noteworthy, the appearance of photoelectric response indirectly proved the formation of V_2O_x/Si heterojunction. But, the poor performance of V_2O_x/Si heterojunction solar cell was attributed to the inferior carrier collection ability.

To further illustrate the formation of V_2O_x/Si heterojunction, the surface potential of V_2O_x/Si cross section was measured by Kelvin probe force microscopy (KPFM) [34,35], and Ag film was sputtered over the V_2O_x film to protect the surface. Fig. 5(a) shows the topography graph of Ag/V_2O_x/Si and the corresponding potential

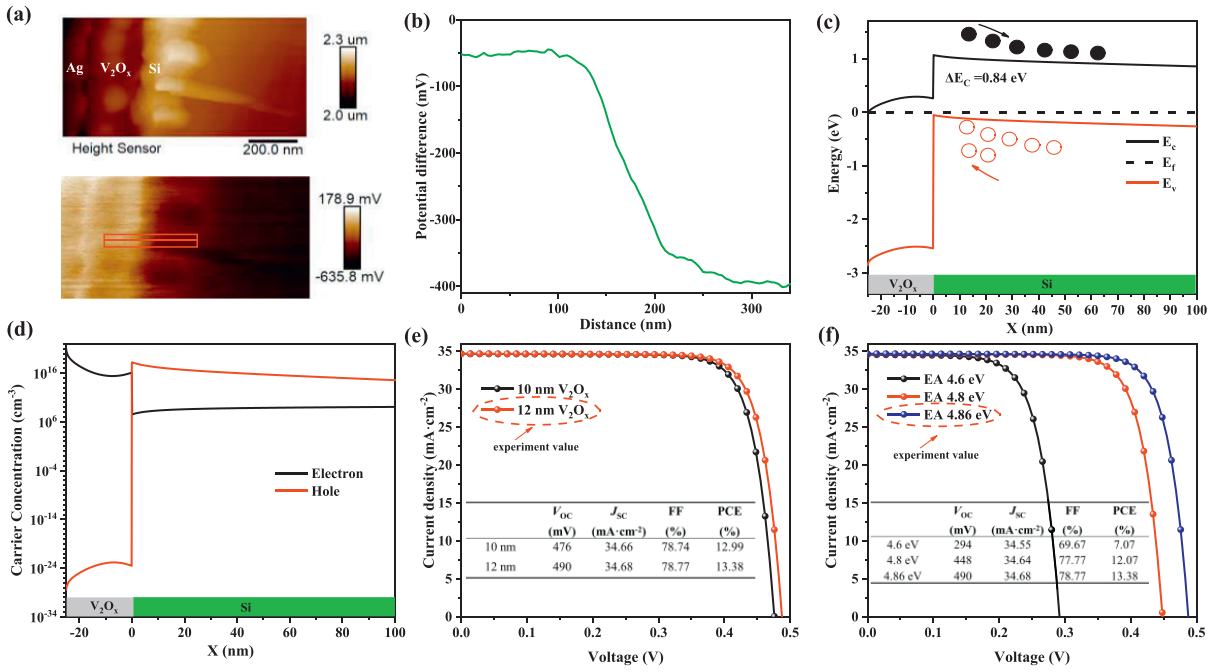

	V_{OC} (mV)	J_{SC} ($mA \cdot cm^{-2}$)	FF (%)	PCE (%)
10 nm	476	34.66	78.74	12.99
12 nm	490	34.68	78.77	13.38

	V_{OC} (mV)	J_{SC} ($mA \cdot cm^{-2}$)	FF (%)	PCE (%)
4.6 eV	294	34.55	69.67	7.07
4.8 eV	448	34.64	77.77	12.07
4.86 eV	490	34.68	78.77	13.38

Fig. 5. Atomic Force Microscope (AFM) images of V_2O_x/Si and heterojunction energy band, carrier concentration information, and performance data of different thicknesses and different electron affinity by simulation. (a) AFM height topography and surface potential image of V_2O_x/Si. (b) Corresponding surface potential difference curve of V_2O_x/Si. (c) V_2O_x/Si heterojunction energy band structure diagram at equilibrium state, and (d) carrier concentration under 0 V bias. (e) Current density-voltage curves at the same electron affinity (EA) of 4.86 eV and different film thicknesses of V_2O_x film at 10 nm, 12 nm. (f) Current density-voltage curves at the same thickness of 12 nm and different EA of V_2O_x film at 4.6, 4.8, and 4.86 eV.

distribution. The surface potential shows the bright and dark areas obviously and has a clear boundary at the V_2O_x/Si interface, which corresponds to a high potential at the V_2O_x film side. The same result was also reflected in Fig. 5(b), at the contact interface of V_2O_x film and Si, the potential dropped sharply about 300 mV. It was also demonstrated that the carrier was effectively separated at the V_2O_x/Si interface. Hence, this also illustrates the formation of heterojunction and aids in explaining the hole accumulation on the high potential side of V_2O_x film after the heterojunction formed.

Meanwhile, the performance and the energy band information of V_2O_x/Si heterojunction solar cell was also demonstrated by numerical simulation to illustrate its high efficiency. First, the model of V_2O_x/Si heterojunction solar cell was constructed, and the thickness of n-Si wafer was set to 300 μm. We use COMSOL Multiphysics 5.6 software, which is based on the finite volume method to calculate the energy band of V_2O_x/Si heterojunction. A one-dimensional silicon solar cell model is constructed, and we select the semiconductor balance in semiconductor module to study. Moreover, we set the doping concentration of Si and V_2O_x, and the Shockley-Read-Hall model is employed to capture the main recombination effect. And then, we select the parameters of Si and V_2O_x, including band gap, electron affinity (EA), and the rear contact was set an ideal ohmic contact. In the simulation model, Schottky contact had been set on the upper layer of V_2O_x. Next, different thickness and EA of V_2O_x film were further controlled to explore the best parameters. Fig. 5 also shows the energy band diagram and carrier concentration of V_2O_x/Si heterojunction solar cell. In Fig. 5(c), the energy band structure diagram at the equilibrium state was shown, at the interface of V_2O_x/Si heterojunction, the band bending appeared about 0.84 eV, which can accelerate carrier separation effectively. The trend was hole through to V_2O_x film from the Si valence band, and the electron was transported to the back electrode. The carrier concentration under 0 V bias was also shown in Fig. 5(d), and it was consistent with previous conclusion; V_2O_x is more likely to be an n-type semiconductor. It was found that, on the V_2O_x film side, electrons are the majority carrier, on the Si side, although the holes are the majority carrier from 0 to 400 nm, after 400 nm, the electrons are the majority carrier in Fig. S5. Therefore, at the interface of V_2O_x/Si heterojunction, the holes are majority carrier; it was demonstrated that the TAT help the holes transport from Si to V_2O_x film.

The thickness and EA of V_2O_x film also influence the performance of V_2O_x/Si heterojunction solar cell. Therefore, we detected different thicknesses and EA of V_2O_x film by the numerical simulation, and the results were shown in Fig. 5(e) and (f). In the experiment, we obtained the film thickness, E_g, and EA was 12 nm, 2.8 eV, and 4.86 eV of V_2O_x film, respectively. Furthermore, the simulation results show that as the thickness increase, the short current density (J_{SC}) almost unchanged, the Fill factor (FF) and V_{OC} were enhanced with the thickness increased of V_2O_x film at the same EA of 4.86 eV. When the thickness is 12 nm, the PCE of V_2O_x/Si heterojunction solar cell was 13.38% in Fig. 5(e). Moreover, with the thickness of V_2O_x film further increased, the PCE was further improved to 14.60% in Fig. S6(a). However, when the thickness of V_2O_x film was 30 nm, the performance was decreased to 14.38% in Table S1. Under the condition of the same thickness of 12 nm, low EA result in the V_{OC}, FF, and PCE was 294 mV, 69.67%, and 7.07%, respectively in Fig. 5(f). With the EA enhanced to 4.86 eV, the V_{OC} and PCE improved obviously. In Fig. S6(b), under the premise of theoretically optimal thickness, the performance of V_2O_x/Si heterojunction solar cell was improved significantly because of the increased EA. Based on the thickness and EA were 25 nm and 5.6 eV of V_2O_x film, the V_{OC} and PCE achieved about 686 mV and 19.90% in Table S2. This illustrated that the V_2O_x/Si heterojunction solar cell has high efficiency under ideal condition.

2.3. Performance improvement of V_2O_x/Si heterojunction solar cell

By analyzing the numerical simulation results, the high efficiency of V_2O_x/Si heterojunction solar cell was shown. However, the performance of V_2O_x/Si heterojunction solar cell was inferior in experiment, which was due to the less favorable lateral conductivity of V_2O_x film, and the separated carrier cannot be collected actively. Thus, we used the assisted carrier collection layer of PEDOT:PSS film to improve the carrier collection efficiency, achieving the performance improved of V_2O_x/Si heterojunction solar cell. In the following discussion, the structure of this solar cell was called assistant V_2O_x/Si heterojunction solar cell. Fig. 6 shows the performance characterization of assistant V_2O_x/Si heterojunction solar cell at different V_2O_x concentrations with 1:150, 1:200, and 1:250, respectively. The short-circuit current difference is because of the different thickness of V_2O_x film with different concentrations. In Fig. 6(a), 1:200 concentration assistant V_2O_x/Si heterojunction solar cell possesses the highest short current density was 29.97 mA/cm^2. The increase in J_{SC} compared to the basic V_2O_x/Si heterojunction solar cell is due to the PEDOT:PSS assisted enhanced carrier collection and reduced surface reflectivity. At 1:150 concentration, the short current density is close to the highest, but at 1:250 concentration, the short current density is the lowest of 28.98 mA/cm^2. Open circuit voltage can be analyzed by formula (2),

$$V_{OC} = \frac{kT}{q} \ln \frac{I_{SC} + I_{01}}{I_{01}} \approx \frac{kT}{q} \ln \frac{I_{SC}}{I_{01}} \quad (2)$$

where k is the Boltzmann constant, T is the absolute temperature, q is the electron power, I_{01} is the dark current, and I_{SC} is the photogenerated current. Fig. 6(d) is the dark current of different concentration V_2O_x solution of assistant V_2O_x/Si heterojunction solar cells. The dark current is lower at the 1:200 solution concentration, which corresponds to the high open circuit voltage. Compared with the basic V_2O_x/Si heterojunction solar cell, the V_{OC} of assistant V_2O_x/Si solar cell was enhanced. According to formula (2), the V_{OC} was also influenced by I_{SC}, when the carrier collection layer has not existed, the separated carrier by V_2O_x/Si heterojunction cannot be collected effectively, and the value of I_{SC} was lower, resulting in the lower V_{OC}. When the assist carrier collection layer was available, the separated carrier could be collected very well by PEDOT:PSS and correctly transported to Ag electrode to converge into current, and increased I_{SC}. Indirectly, it also can decrease the recombination of carrier at Ag and V_2O_x interface. Therefore, the good carrier collection effect increased I_{SC} and enhanced V_{OC} of assistant V_2O_x/Si heterojunction solar cells.

The external quantum efficiency (*EQE*) is defined as the probability that one electron is available to the outside for each incident photon of wavelength λ for the entire incident solar spectrum. *EQE* can be expressed by the following equation:

$$EQE(\lambda) = \frac{J_{SC}(\lambda)}{qQ(\lambda)} \quad (3)$$

where $Q(\lambda)$ is the incident photon energy density, and *EQE* is shown in Fig. 6(b). It can be concluded that in the wavelength range from 300 to 500 nm, the 1:200 concentration assistant V_2O_x/Si heterojunction solar cell has the highest *EQE*. Around 500–1000 nm, the *EQE* of the 1:150 concentration assistant V_2O_x/Si heterojunction solar cell is gradually enhanced to the same level as the 1:200 concentration assistant V_2O_x/Si heterojunction solar cell, which exhibits good response in long wavelength range. However, at 800–1000 nm wavelength, the *EQE* of the 1:250 concentration assistant V_2O_x/Si heterojunction solar cell is lower than that of

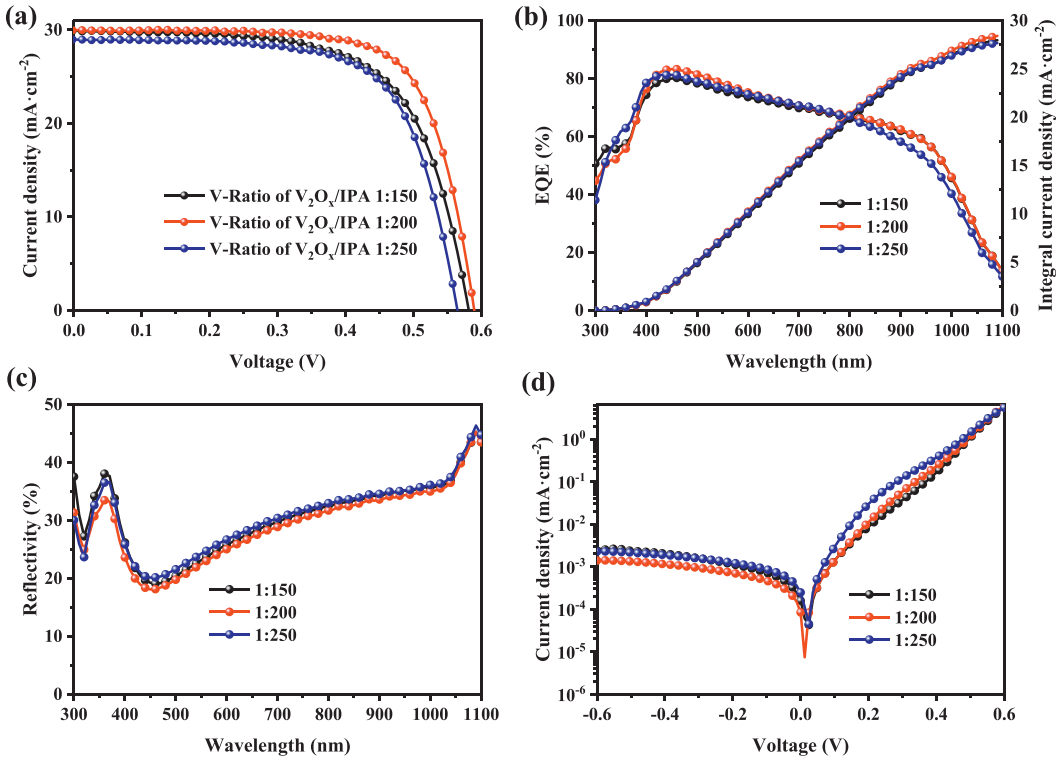

Fig. 6. Performance data of PEDOT:PSS/V_2O_x/Si heterojunction solar cells under different V_2O_x solution concentrations. (a) Current density-voltage curves and (b) *EQE*, integral current density, (c) reflectivity spectra, and (d) current density-voltage curves without light of PEDOT:PSS/V_2O_x/Si heterojunction solar cells under different V_2O_x solution concentrations of 1:150, 1:200 and 1:250.

Table 3
Electrical output parameters of V_2O_x/Si heterojunction solar cells.

	V_{OC} (mV)	J_{SC} (mA/cm^2)	FF (%)	PCE (%)
1:150	579 (583 ± 3.8)	29.91 (29.71 ± 0.14)	65.43 (65.63 ± 0.4)	11.33 (11.37 ± 0.05)
1:200	593 (591 ± 3.1)	29.97 (30.22 ± 0.29)	71.12 (70.7 ± 0.07)	12.64 (12.65 ± 0.08)
1:250	565 (565 ± 0)	28.98 (29.11 ± 0.22)	67.66 (67.63 ± 0.8)	11.08 (11.12 ± 0.08)

*The data in parentheses are calculated by five sets of solar cells.

1:150 and 1:200 concentration. Meanwhile, the integral current density was also shown the same change with J_{SC}. In Fig. 6(c), the reflectivity of three kinds of assistant V_2O_x/Si heterojunction solar cell were also displayed, and it shows the lowest reflectivity of 1:200 concentration and corresponds the J_{SC} change.

The electrical output parameters of assistant V_2O_x/Si heterojunction solar cells are shown in Table 3. 1:200 concentration assistant V_2O_x/Si heterojunction solar cell has the highest fill factor of 71.12%, which makes the quality of assistant V_2O_x/Si heterojunction solar cell improved. The PCE of assistant V_2O_x/Si heterojunction solar cell can be obtained according to the following formula:

$$\eta = \frac{P_{mp}}{P_{in}} = FF \cdot J_{SC} \cdot V_{OC} \quad (4)$$

where η is PCE, P_{mp} is the maximum output power and P_{in} is the incident power. It can be obtained by multiplying the value of FF, J_{SC} and V_{OC}. Finally, the PCE of the assistant V_2O_x/Si heterojunction solar cell is 12.64%.

3. Conclusion

We achieved the assembly of the V_2O_x/Si heterojunction and demonstrated the formation of heterojunction by KPFM with the potential difference between V_2O_x and Si contact interface. In order to enhance the carrier collection efficiency, PEDOT:PSS was introduced as an assist carrier collection layer on the front surface. It was also found that, with the increasing of annealing temperature, the valence state of V in V_2O_x changes, and the content of V^{5+} gradually increases, the content of V^{4+} gradually decreases. The valence band energy level position, work function, and EA were 7.66 eV, 4.93 eV, and 4.86 eV, respectively, and the energy band contact properties of forming heterojunction with Si were beneficial for carrier separation. The V_2O_x/Si heterojunction solar cells were also fabricated, and the numerical simulation displayed that the high band bending accelerates the carrier separation. The PCE of V_2O_x/Si heterojunction solar cell was 14.60%; under the condition, EA and thickness was 4.86 eV and 25 nm. Ultimately, PEDOT:PSS film was used to assist in enhancing carrier collection efficiency, accomplished a PCE of 12.64% in experiment.

4. Experimental section

4.1. Materials

Radial (100) polished single-side n-Si wafer was purchased from Tianjin Upward Technology Development Co., Ltd., with the resistivity and thickness was 2–4 Ω cm and 500 μm. PEDOT:PSS solution is Clevios PH1000 of Heraeus. Triton® X-100 (TX-100) and ethylene glycol, 99%, were purchased from Alfa and Innochem. Triisopropoxyvanadium(V) oxide and isopropyl alcohol were purchased from TCI and Aladdin.

4.2. V_2O_x/Si heterojunction solar cell fabrication

The Si wafer was cut into 1 × 1 cm^2 by laser dicing machine. And then the Si wafer was cleaned in acetone, ethanol, and deionized (DI) water for 10 min each, and dry the Si wafer with nitrogen. After cleaning process, the 5% hydrofluoric acid was used to remove the native oxide layer on Si surface and then cleaned with DI water; 5 wt% EG and 0.25 wt% TX-100 were mixed with PEDOT:PSS solution and stirred adequately. First, 200 μl triisopropoxyvanadium(V) oxide was added into 2000 μl isopropanol to prepare a precursor solution with a concentration of 1:10, open and fully stir at room temperature. And then, three groups of solutions were further configured respectively. Group 1, 20 μl precursor solution was added into 3000 μl isopropanol to form a concentration of 1:150 solution. Group 2, 20 μl precursor solution was added into 4000 μl isopropanol to form a concentration of 1:200 solution. Group 3, 20 μl precursor solution was added into 5000 μl isopropanol to form a concentration of 1:250 solution. The all solution was in an open container stir 2 h. Different concentrations of V_2O_x solution were spin coated onto front Si surface at 4000 rpm. After that, the PEDOT:PSS solution was spin coated onto front sample surface at 4000 rpm and then annealed at 120 °C for 15 min. Ag electrode was deposited onto the PEDOT:PSS film through a shadow mask by magnetron sputtering with a thickness of 200 nm. An Ag film was prepared as rear electrode with a thickness of 100 nm. Finally, the solar cell was cut into 0.5 × 0.5 cm^2 for testing.

4.3. Characterization

The solar simulator (Keithley 2400, AM 1.5G, 100 mW/cm^2) was used to test the current density and voltage (J-V) characteristics. The morphology and surface potential of V_2O_x film were characterized by Hitachi SU8010 cold field SEM and BRUKER ICON (AFM). The crystallinity of V_2O_x films and Raman spectrum on Si substrate at different temperatures was examined by XRD (Empyrean) and Raman (LabRAM Odyssey). XPS and UPS were used to measure the optoelectronic information of V_2O_x films. The Enli technology QE-R test system was used to detect EQE spectra and reflectivity spectra. The optical properties of V_2O_x films on FTO were obtained by UV2600i.

Credit author statement

Geng Qi, Wang Zhe, Liu Zhen, Liu Yuzhou: Software, Writing – Original draft preparation. **Gao Zhongliang:** Conceptualization, Methodology. **Li Yingfeng, Sun Xin, Chen Lei, Lv Xiaojun:** Investigation. **Li Meicheng:** Conceptualized the idea, Discussed the results, Reviewed, Supervised.

Declaration of competing interest

The authors declare that they have no known competing financial interests or personal relationships that could have appeared to influence the work reported in this paper.

Data availability

Data will be made available on request.

Acknowledgment

This work is supported partially by National Natural Science Foundation of China (Grant nos. 52232008, 51972110, 52102245, and 52072121), Beijing Natural Science Foundation (2222076, 2222077), Beijing Science and Technology Project (Z211100004621010), project of State Key Laboratory of Alternate Electrical Power System with Renewable Energy Sources (LAPS202114), 2022 Strategic Research Key Project of Science and Technology Commission of the Ministry of Education, Huaneng Group Headquarters Science and Technology Project (HNKJ20-H88), Youth Innovation Team Development Plan of Colleges and Universities in Shandong Province (2022KJD007), the Fundamental Research Funds for the Central Universities (2022MS029, 2022MS02, 2022MS031) and the NCEPU "Double First-Class" Program.

Appendix A. Supplementary data

Supplementary data to this article can be found online at https://doi.org/10.1016/j.mtener.2023.101317.

References

[1] L.G. Gerling, S. Mahato, A. Morales-Vilches, G. Masmitja, P. Ortega, C. Voz, R. Alcubilla, J. Puigdollers, Transition metal oxides as hole-selective contacts in silicon heterojunctions solar cells, Sol. Energy Mater. Sol. Cells 145 (2016) 109–115.

[2] O. Almora, L.G. Gerling, C. Voz, R. Alcubilla, J. Puigdollers, G. Garcia-Belmonte, Superior performance of V_2O_5 as hole selective contact over other transition metal oxides in silicon heterojunction solar cells, Sol. Energy Mater. Sol. Cells 168 (2017) 221–226.

[3] C.-Y. Chen, T.-C. Wei, P.-H. Hsiao, C.-H. Hung, Vanadium oxide as transparent carrier-selective layer in silicon hybrid solar cells promoting photovoltaic performances, ACS Appl. Energy Mater. 2 (2019) 4873–4881.

[4] G. Masmitjà, L.G. Gerling, P. Ortega, J. Puigdollers, I. Martín, C. Voz, R. Alcubilla, V_2O_x-based hole-selective contacts for c-Si interdigitated back-contacted solar cells, J. Mater. Chem. 5 (2017) 9182–9189.

[5] T. Lei, H. Dong, J. Xi, Y. Niu, J. Xu, F. Yuan, B. Jiao, W. Zhang, X. Hou, Z. Wu, Highly-efficient and low-temperature perovskite solar cells by employing a Bi-hole transport layer consisting of vanadium oxide and copper phthalocyanine, Chem. Commun. 54 (2018) 6177–6180.

[6] Z. Liu, T. He, K. Liu, Q. Zhi, M. Yuan, Solution processed double-decked V_2O_x/PEDOT:PSS film serves as the hole transport layer of an inverted planar perovskite solar cell with high performance, RSC Adv. 7 (2017) 26202–26210.

[7] Z. Liu, T. He, H. Wang, X. Song, H. Liu, J. Yang, K. Liu, H. Ma, Improving the stability of the perovskite solar cells by V_2O_5 modified transport layer film, RSC Adv. 7 (2017) 18456–18465.

[8] M.M. Tepliakova, A.N. Mikheeva, L.A. Frolova, A.G. Boldyreva, A. Elakshar, A.V. Novikov, S.A. Tsarev, M.I. Ustinova, O.R. Yamilova, A.G. Nasibulin, S.M. Aldoshin, K.J. Stevenson, P.A. Troshin, Incorporation of vanadium(V) oxide in hybrid hole transport layer enables long-term operational stability of perovskite solar cells, J. Phys. Chem. Lett. 11 (2020) 5563–5568.

[9] S.-P. Cho, J.-S. Yeo, D.-Y. Kim, S.-i. Na, S.-S. Kim, Brush painted V_2O_5 hole transport layer for efficient and air-stable polymer solar cells, Sol. Energy Mater. Sol. Cells 132 (2015) 196–203.

[10] J. Kim, H. Kim, G. Kim, H. Back, K. Lee, Soluble transition metal oxide/polymeric acid composites for efficient hole-transport layers in polymer solar cells, ACS Appl. Mater. Interfaces 6 (2014) 951–957.

[11] J. Pan, P. Li, L. Cai, Y. Hu, Y. Zhang, All-solution processed double-decked PEDOT:PSS/V_2O_5 nanowires as buffer layer of high performance polymer photovoltaic cells, Sol. Energy Mater. Sol. Cells 144 (2016) 616–622.

[12] K. Zilberberg, S. Trost, H. Schmidt, T. Riedl, Solution processed vanadium pentoxide as charge extraction layer for organic solar cells, Adv. Energy Mater. 1 (2011) 377–381.

[13] F. Xie, W.C. Choy, C. Wang, X. Li, S. Zhang, J. Hou, Low-temperature solution-processed hydrogen molybdenum and vanadium bronzes for an efficient hole-transport layer in organic electronics, Adv. Mater. 25 (2013) 2051–2055.

[14] G. Terán-Escobar, J. Pampel, J.M. Caicedo, M. Lira-Cantú, Low-temperature, solution-processed, layered V2O5 hydrate as the hole-transport layer for stable organic solar cells, Energy Environ. Sci. 6 (2013) 3088–3098.

[15] N.-W. Teng, C.-H. Li, W.-C. Lo, Y.-S. Tsai, C.-Y. Liao, Y.-W. You, H.-L. Ho, W.-L. Li, C.-C. Lee, W.-C. Lin, Y.-M. Chang, Highly efficient nonfullerene organic photovoltaic devices with 10% power conversion efficiency enabled by a fine-tuned and solution-processed hole-transporting layer, Solar RRL 4 (2020), 2000223.

[16] K. Gao, Q. Bi, X. Wang, W. Liu, C. Xing, K. Li, D. Xu, Z. Su, C. Zhang, J. Yu, D. Li, B. Sun, J. Bullock, X. Zhang, X. Yang, Progress and future prospects of wide-bandgap metal-compound-based passivating contacts for silicon solar cells, Adv. Mater. 34 (2022), e2200344.

[17] J. Dréon, Q. Jeangros, J. Cattin, J. Haschke, L. Antognini, C. Ballif, M. Boccard, 23.5%-efficient silicon heterojunction silicon solar cell using molybdenum oxide as hole-selective contact, Nano Energy 70 (2020), 104495.

[18] X.B. Yang, H. Xu, W.Z. Liu, Q.Y. Bi, L.J. Xu, J.X. Kang, M.N. Hedhili, B.Q. Sun, X.H. Zhang, S. De Wolf, Atomic layer deposition of vanadium oxide as hole-selective contact for crystalline silicon solar cells, Adv. Energy Mater. 6 (2020), 2000467.

[19] G. Du, L. Li, H. Zhu, L. Lu, X. Zhou, Z. Gu, S.T. Zhang, X. Yang, J. Wang, L. Yang, X. Chen, D. Li, High-performance hole-selective V_2O_X/SiO_X/NiO_X contact for crystalline silicon solar cells, EcoMat 4 (2022), e12175.

[20] S.-H. Kim, J.-Y. Jung, R.B. Wehrspohn, J.-H. Lee, All-room-temperature processed 17.25%-crystalline silicon solar cell, ACS Appl. Energy Mater. 3 (2020) 3180–3185.

[21] G.L. Du, L. Li, X.B. Yang, X. Zhou, Z.H. Su, P.H. Cheng, Y.Y. Lin, L.F. Lu, J.L. Wang, L.Y. Yang, X.Y. Gao, X.Y. Chen, D.D. Li, Improved V_2O_X passivating contact for p-type crystalline silicon solar cells by oxygen vacancy modulation with a SiO_X tunnel layer, Adv. Mater. Interfaces 8 (2021), 2100989.

[22] T. Sun, R.B. Wang, R.Y. Liu, C. Wu, Y.N. Zhong, Y.Q. Liu, Y.S. Wang, Y.J. Han, Z.H. Xia, Y.T. Zou, T. Song, N. Koch, S. Duhm, B.Q. Sun, Investigation of MoO_x/n-Si strong inversion layer interfaces via dopant-free heterocontact, Phys. Status Solidi Rapid Res. Lett. 11 (2017), 1700107.

[23] C. Lu, Rusli, A.B. Prakoso, H. Wang, Hole selective WO_x and V_2O_x contacts using solution process for silicon solar cells application, Mater. Chem. Phys. 273 (2021), 125101.

[24] G. Ma, R. Du, Y.-n. Cai, C. Shen, X. Gao, Y. Zhang, F. Liu, W. Shi, W. Du, Y. Zhang, Improved power conversion efficiency of silicon nanowire solar cells based on transition metal oxides, Sol. Energy Mater. Sol. Cells 193 (2019) 163–168.

[25] G.Y. Song, C. Oh, S. Sinha, J. Son, J. Heo, Facile phase control of multivalent vanadium oxide thin films (V_2O_5 and VO_2) by atomic layer deposition and postdeposition annealing, ACS Appl. Mater. Interfaces 9 (2017) 23909–23917.

[26] R. Baddour-Hadjean, J.P. Pereira-Ramos, C. Navone, M. Smirnov, Raman microspectrometry study of electrochemical lithium intercalation into sputtered crystalline V_2O_5 thin films, Chem. Mater. 20 (2008) 1916–1923.

[27] C.V. Ramana, R.J. Smith, O.M. Hussain, M. Massot, C.M. Julien, Surface analysis of pulsed laser deposited V_2O_5 thin films and their lithium intercalated products studied by Raman spectroscopy, Surf. Interface Anal. 37 (2005) 406–411.

[28] M. Kang, J. Jung, S.-Y. Lee, J.-W. Ryu, S.W. Kim, Conductivity, carrier density, mobility, Seebeck coefficient, and power factor in V_2O_5, Thermochim. Acta 576 (2014) 71–74.

[29] J. Tong, Y. Wan, J. Cui, S. Lim, N. Song, A. Lennon, Solution-processed molybdenum oxide for hole-selective contacts on crystalline silicon solar cells, Appl. Surf. Sci. 423 (2017) 139–146.

[30] D. Manno, A. Serra, M. Di Giulio, G. Micocci, A. Taurino, A. Tepore, D. Berti, Structural and electrical properties of sputtered vanadium oxide thin films for applications as gas sensing material, J. Appl. Phys. 81 (1997) 2709–2714.

[31] M.A. Abdelhameed, Mostafa F. Esmat, Jevasuwan Mohamed, Wipakorn Fukata, Naoki, Hole-injection role of solution-processed thermally treated VOx thin films in Si nanowire-based solar cells, Nano Energy 99 (2022), 107373.

[32] K. Zilberberg, S. Trost, J. Meyer, A. Kahn, A. Behrendt, D. Lützenkirchen-Hecht, R. Frahm, T. Riedl, Inverted organic solar cells with sol-gel processed high work-function vanadium oxide hole-extraction layers, Adv. Funct. Mater. 21 (2011) 4776–4783.

[33] C. Messmer, M. Bivour, J. Schon, S.W. Glunz, M. Hermle, Numerical simulation of silicon heterojunction solar cells featuring metal oxides as carrier-selective contacts, IEEE J. Photovolt. 8 (2018) 456–464.

[34] Z. Liang, M. Su, H. Wang, Y. Gong, F. Xie, L. Gong, H. Meng, P. Liu, H. Chen, W. Xie, J. Chen, Characteristics of a silicon nanowires/PEDOT:PSS heterojunction and its effect on the solar cell performance, ACS Appl. Mater. Interfaces 7 (2015) 5830–5836.

[35] P. Cui, D. Wei, J. Ji, H. Huang, E. Jia, S. Dou, T. Wang, W. Wang, M. Li, Planar p–n homojunction perovskite solar cells with efficiency exceeding 21.3, Nat. Energy 4 (2019) 150–159.